Journal of Advances in Mathematics and Computer Science

23(2): 1-16, 2017; Article no.JAMCS.34292

Previously known as British Journal of Mathematics & Computer Science
ISSN: 2231-0851

Effects of Radiation and Chemical Reaction on MHD Unsteady Heat and Mass Transfer of Casson Fluid Flow Past a Vertical Plate

R. Biswas[1*], M. Mondal[1], D. R. Sarkar[1] and S. F. Ahmmed[1*]

[1]Mathematics Discipline, Khulna University, Khulna, Bangladesh.

Authors' contributions

This work was carried out in collaboration between all authors. Author RB designed the study, performed the statistical analysis, wrote the protocol and wrote the first draft of the manuscript. Author MM managed the analyses of the study and author DRS managed the literature searches. Author SFA formulated the finite difference method code in FORTRAN language, edited the manuscript and gave the overall guidance for the study. All authors read and approved the final manuscript.

Article Information

DOI: 10.9734/JAMCS/2017/34292
Editor(s):
(1) Kai-Long Hsiao, Taiwan Shoufu University, Taiwan.
Reviewers:
(1) Animasaun, Isaac L., Federal University of Technology, Akure, Ondo State, Nigeria.
(2) Bhim Sen Kala, K. L. University, Vaddesawaram, Guntur, A.P., India.
(3) Hunegnaw Dessie, Debre Markos University, Ethiopia.
Complete Peer review History: http://www.sciencedomain.org/review-history/19926

Original Research Article

Received: 22nd May 2017
Accepted: 28th June 2017
Published: 7th July 2017

Abstract

Effects of radiation and chemical reaction on MHD unsteady heat and mass transfer of Casson fluid flow past a vertical plate has been studied in this paper. The model equations are transformed into non-dimensional form by the as usual mathematical technique of transformation and the resultant non-dimensional partial differential equations are solved by using explicit finite difference method. The obtained results are plotted after stability test by using graphics software TECPLOT-9. The results are showed for various dimensionless parameters such as Casson parameter, Permeability of porous medium, Schmidt number, Grashof number, Prandtl number, Chemical reaction and Radiation parameter on velocity, temperature and concentration profiles along with the local skin friction, local Nusselt number and Sherwood number with the help of computer programming languages COMPAQ VISUAL FORTRAN 6.6a. The results are discussed with the help of graphs. Finally, we obtained that velocity decrease with an increase in Casson parameter, Permeability of porous medium and Chemical reaction while it increase with increasing values of Radiation parameter and Grashof number. Temperature increase due to Radiation parameter but decrease for Prandtl number. Therefore, the results of the present problem have an excellent agreement with the results of Raju et al. [2].

**Corresponding authors: E-mail: rajibkumath11@gmail.com, sfahmmed@yahoo.com;*

Keywords: Casson fluid; chemical reaction; radiation parameter; MHD; porous medium.

1 Introduction

The study of Casson fluid flow particularly in the magneto-hydrodynamic effect with heat and mass transfer has been received considerable attention to many researchers in last few years. In addition, magneto-hydrodynamic (MHD) is the branch of continuum mechanics which deals with the flow of electrically conducting fluid in electrical and magnetic fields. The flow of an electrically conducting fluid in the presence of a magnetic field is important in various area of technology. There are many applications of MHD free convection flows in fiber and granular insulation, geothermal systems etc. Throughout the last few decades a great deal of research work have been done about the magneto-hydrodynamic effects of Casson fluid flow, Hall current, Radiation and Chemical reaction through porous plate.

Casson fluid is a Rheopectic type non-Newtonian fluid when shear force is applied then its viscosity will be increases. Such as gypsum paste, cream etc. Sojoudi et al. [1] presented similarity solutions for flow and heat transfer of non-Newtonian fluid over a stretching surface. It is observed from their work, they used similarity solutions to solve their problem. Also, they obtained ordinary differential equations which are solved numerically by using the shooting method. Raju et al. [2] illustrated heat and mass transfer in magneto-hydrodynamic Casson fluid over an exponentially permeable stretching surface. They have described the effects of different parameters on velocity, temperature and concentration profiles. Soret and heat generation effects on MHD Casson fluid flow past an oscillating vertical plate embedded through porous medium have been studied by Kataria and Patel [3]. They discussed about analytical solutions. Also, they used Laplace transform and numerical solution to solved their problem where they used matlab software (finite difference method) of the unsteady natural convective Casson fluid flow past over an oscillating vertical plate in the presence of a radiation, chemical reaction, thermal diffusion and heat generation with ramped wall temperature and ramped surface concentration through porous medium. Oyelakin et al. [4] studied about unsteady Casson nanofluid flow over a stretching sheet with thermal radiation, convective and slip boundary conditions. Animasaun [5] studied effects of thermophoresis, variable viscosity and thermal conductivity on free convective heat and mass transfer of non-darcian MHD dissipative Casson fluid flow with suction and nth order of chemical reaction. Casson fluid flow with variable thermo-physical property along exponentially stretching sheet with suction and exponentially decaying internal heat generation using the homology analysis method have been presented by Animasaun et al. [6]. Ahmed et al. [7] studied about the effects on magnetic field in squeezing flow of a Casson fluid between parallel plates. Similarity solution of 3D Casson nanofluid flow over a stretching sheet with convective boundary conditions have introduced by Sulochana et al. [8].

Magneto-hydrodynamics (MHD) deals with the flow of electrically conducting fluids in electric and magnetic fields which is a branch of magneto fluid dynamics. This phenomenon on most likely comes from the field of astrophysics. In the universe, most of the matters are in the plasma or highly ionized gaseous state and in the region of electromagnetic fluid dynamics much of the basic knowledge evolved from these studies. The study of a continuous, electrically conducting fluid under the influence of electromagnetic fields is consisted by the field of Magneto-hydrodynamics. MHD free convection and mass transfer flow through a vertical oscillatory porous plate with Hall, ion-slip currents and heat source in a rotating system have been presented by Hossain et al. [9]. Hall effects on unsteady MHD free convective flow past an accelerated moving vertical plate with viscous and joule dissipations have been studied by Sarkar et al. [10]. They used Crank-Nicolsons implicit technique with tri-diagonal matrix manipulation and iterative procedure to solve their problem. Also, they showed the effects of different parameters on velocity, temperature and concentration respectively. Effects of hall current, radiation and rotation on natural convection heat and mass transfer flow past a moving vertical plate illustrated by Seth et al. [11]. They observed, Dufour effect has been consider in energy equation leaving the equations of thermal diffusion and mass diffusion coupled. Pattnaik et al. [12] presented diffusion- thermo effect with hall current on unsteady hydromagnetic flow past an infinite vertical porous plate. It is observed from their work that the velocity decreases with the increases of both suction and injection. Hossain et al. [13] studied about combined convection from a vertical flat plate

with temperature dependent viscosity and thermal conductivity. Magneto-hydrodynamic flow of Casson fluid over a stretching cylinder have been studied by Tamoor et al. [14]. Das et al. [15] presented Hall effects on an unsteady magneto-convection and radiative heat transfer past a porous plate. They solved their governing equations by using fourth order Runge-Kutta- Fehlberg method with the shooting technique. They have described the effects of different parameters on flow field, temperature distribution, shear stresses and rate of heat transfer at the plate.

A chemical reaction is processed that leads to the transformation of one set of chemical substances to another. The most common fluid fluids like water and air are contaminated with impurities like CO_2, C_6H_6 and H_2SO_4 etc. When such contaminant is present in the fluid under consideration there takes place some chemical reaction e.g. air and benzene react chemically, so also water and sulphuric acid. Chemical reaction and soret effects on hydromagnetic micropolar fluid along a stretching sheet have been studied by Mishra et al. [16]. They have described the effects of different parameters on velocity, temperature and concentration profiles. Finite difference solution of MHD mixed convection flow with heat generation and chemical reaction have been studied by Ahmed and Alam [17]. They obtained non-similar momentum, energy and concentration equations and they solved their problem by finite difference technique. Radiation and chemical reaction effects on MHD Casson fluid flow past an oscillating vertical plate embedded in porous medium studied by Kataria and Patel [18]. Effects of variable permeability and radiation absorption on magneto hydrodynamic (MHD) mixed convective flow in a vertical wavy channel with traveling thermal waves have been presented by Narayanan [19]. Tripathy et al. [20] illustrated chemical reaction effect on MHD free convective surface over a moving vertical plate through porous medium. It is observed from their work that, they have been transformed their governing equations into a two-point boundary value problem using similarity variables and then solved numerically by forth order Runge-Kutta fourth order method with shooting technique.

The main objective of the present paper is to study the effects of radiation and chemical reaction on MHD unsteady heat and mass transfer of Casson fluid flow past a vertical plate. We have extended the work of Raju et al. [2]. They have deliberated steady case in their experimental work but we have considered unsteady case in our present paper. They have used similarity transformation to reduce the governing equations in non-dimensional form and solved numerically their non-dimensional governing equations by using Matlab bvp4c package but we have used a usual transformation in our experiment and solve our problem numerically by using explicit finite different method. Also, we expanded their governing equations with Hall current, joule heating and porous medium terms in our problem. The results are computed for various physical parameters such as Casson parameter, magnetic parameter, Schmidt number, Grashof number, Prandtl number, chemical reaction, radiation parameter etc. with the help of computer programming languages COMPAQ VISUAL FORTRAN 6.6a and the obtained results are plotted after stability test by using graphics software TECPLOT-9. At last, we have shown a comparison table of the accuracy of the present results with the previous results of Raju et al. [2].

2 Mathematical Analysis

We consider the unsteady MHD Casson fluid flow of an electrically conducting viscous incompressible fluid, occupying a semi-infinite region of the shape bounded by an infinite vertical porous permeable plate under the influence of radiation and chemical reaction. The physical model is shown in Fig. 1. In this research work, x-axis is taken along the plate and the y-axis normal to it. It is assume that a uniform magnetic field strength B is applied transversely to the direction of the flow and induced magnetic field strength has ignored. So that $B=(0, B_0, 0)$ and the magnetic lines of forces are fixed relative to the fluid. Initially, it is considered that the plate has the same temperature T_w and concentration C_w level at all points. But at time $t>0$, the plate is accelerated with a velocity $u=U_0$ in its own plane and the temperature and concentration level of the plate are raised linearly to T_∞ and C_∞ with time t.

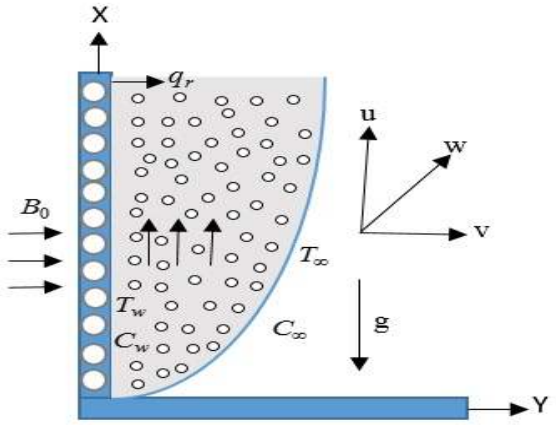

Fig. 1. Physical model and coordinate system

According to Animasaun et al. [6], the rheological equation of state for an isotropic and incompressible flow of Casson fluid is as follows:

$$T_{ij} = \left(\mu_b + \frac{P_y}{\sqrt{2\pi}}\right)2e_{ij} \quad \text{when } \pi > \pi_c \tag{1}$$

$$T_{ij} = \left(\mu_b + \frac{P_y}{\sqrt{2\pi}}\right)2e_{ij} \quad \text{when } \pi < \pi_c \tag{2}$$

Where, P_y is known as yield stress of the fluid, π is Product of the component of deformation rate with itself, e_{ij} is (i, j)th component of the deformation rate, π_c is critical value based on the non-Newtonian model. Under these assumptions along with boundary layer approximation and using Darcy-Forchheimer model, the present problem is governed by following dimensional continuity, first momentum, second momentum, temperature and concentration equations;

$$\frac{\partial u}{\partial x} + \frac{\partial v}{\partial y} = 0 \tag{3}$$

$$\frac{\partial u}{\partial t} + u\frac{\partial u}{\partial x} + v\frac{\partial u}{\partial y} = \upsilon\left(1+\frac{1}{\beta}\right)\frac{\partial^2 u}{\partial y^2} + g\beta_T\left(T-T_\infty\right) + g\beta_C\left(C-C_\infty\right) - \left(1+\frac{1}{\beta}\right)\frac{\upsilon}{k}u - \frac{\sigma B_0^2\left(u+mw\right)}{\rho\left(1+m^2\right)} \tag{4}$$

$$\frac{\partial w}{\partial t} + u\frac{\partial w}{\partial x} + v\frac{\partial w}{\partial y} = \upsilon\left(1+\frac{1}{\beta}\right)\frac{\partial^2 w}{\partial y^2} - \left(1+\frac{1}{\beta}\right)\frac{\upsilon}{k}w - \frac{\sigma B_0^2\left(w-mu\right)}{\rho\left(1+m^2\right)} \tag{5}$$

$$\frac{\partial T}{\partial t} + u\frac{\partial T}{\partial x} + v\frac{\partial T}{\partial y} = \frac{k}{\rho C_p}\frac{\partial^2 T}{\partial y^2} - \frac{1}{\rho C_p}\frac{\partial q_r}{\partial y} + \frac{\sigma B_0^2}{\rho C_p\left(1+m^2\right)}\left(u^2+w^2\right) + \frac{Q}{\rho C_p}\left(T-T_\infty\right)$$

$$+ \frac{D_m k_T}{C_S C_P}\frac{\partial^2 C}{\partial y^2} + \frac{\mu}{\rho C_P}\left(1+\frac{1}{\beta}\right)\left[\left(\frac{\partial u}{\partial y}\right)^2 + \left(\frac{\partial w}{\partial y}\right)^2\right] + \frac{Q}{\rho C_p}\left(C-C_\infty\right) + \frac{\sigma B_0^2 u^2}{\rho C_p} \tag{6}$$

$$\frac{\partial C}{\partial t}+u\frac{\partial C}{\partial x}+v\frac{\partial C}{\partial y}=D_m\frac{\partial^2 C}{\partial y^2}-K_1(C-C_\infty)+\frac{D_m K_T}{T_m}\frac{\partial^2 C}{\partial y^2} \tag{7}$$

The associate initial and boundary conditions according to the problem are,

$$\left.\begin{array}{ll} u=0, v=0, w=0, T=T_w, C=C_w & \text{at } y=0 \\ u=0, v=0, w=0, T\to T_\infty, C\to C_\infty & \text{as } y\to\infty \end{array}\right\} \tag{8}$$

Here, *u*, *v* and *w* are the velocity components in the *x*, *y* and *z*-axis respectively, υ is the kinematic viscosity, C_p is the specific heat, K_T is the thermal conductivity, ρ is the fluid density, *T* is the temperature of fluid, τ is the time constant and q_r is the radiated heat flux. By the Rosseland approximation which is defined as

$$q_r=-\frac{4\sigma}{3k}\frac{\partial T^4}{\partial y} \tag{9}$$

where, σ is the Slefan-Boltzmann constant. Expanding T^4 by Taylor series as

$$T^4\approx T_\infty^4+4T_\infty^3T-4T_\infty^3T_\infty\approx 4T_\infty^3T-3T \tag{10}$$

Since the solution of the governing equations under the initial and boundary conditions have been based on the finite difference method. It is to be required to make the equations dimensionless. For this purpose the following dimensionless variables are used.

$$U=\frac{u}{U_0};\ V=\frac{v}{U_0};\ W=\frac{w}{U_0};\ Y=\frac{yU_0}{\upsilon};\ X=\frac{xU_0}{\upsilon};\ \tau=\frac{tU_0^2}{\upsilon}$$

$$T=T_\infty+\overline{T}(T_w-T_\infty);\quad C=C_\infty+\overline{C}(C_w-C_\infty)$$

where, U, W, $\overline{T}$ and $\overline{C}$ represents the dimensionless primary velocity, secondary velocity, fluid temperature and fluid concentration respectively. Now we substitute the values of the above derivatives into the equations (3) to (7) and simplifying we obtain the following nonlinear coupled partial differential equations in terms of dimensionless variables.

$$\frac{\partial U}{\partial X}+\frac{\partial U}{\partial Y}=0 \tag{11}$$

$$\frac{\partial U}{\partial \tau}+U\frac{\partial U}{\partial X}+V\frac{\partial U}{\partial Y}=\left(1+\frac{1}{\beta}\right)\frac{\partial^2 U}{\partial Y^2}+G_r\overline{T}+G_m\overline{C}-M\frac{U+mW}{1+m^2}-\left(1+\frac{1}{\beta}\right)K_pU \tag{12}$$

$$\frac{\partial W}{\partial \tau}+U\frac{\partial W}{\partial X}+V\frac{\partial W}{\partial Y}=\left(1+\frac{1}{\beta}\right)\frac{\partial^2 W}{\partial Y^2}-M\frac{W-mU}{1+m^2}-\left(1+\frac{1}{\beta}\right)K_pW \tag{13}$$

$$\frac{\partial \overline{T}}{\partial \tau}+U\frac{\partial \overline{T}}{\partial X}+V\frac{\partial \overline{T}}{\partial Y}=\frac{1}{P_r}\frac{\partial^2 \overline{T}}{\partial Y^2}+R_a\frac{\partial^2 \overline{T}}{\partial Y^2}+\frac{E_cM}{(1+m^2)}(U^2+W^2)+\alpha\overline{T}+D_u\frac{\partial^2 \overline{C}}{\partial Y^2}$$

$$+E_c\left(1+\frac{1}{\beta}\right)\left(\frac{\partial U}{\partial Y}\right)^2+E_c\left(1+\frac{1}{\beta}\right)\left(\frac{\partial W}{\partial Y}\right)^2+Q\overline{C}+E_cMU^2 \tag{14}$$

$$\frac{\partial \overline{C}}{\partial \tau}+U\frac{\partial \overline{C}}{\partial X}+V\frac{\partial \overline{C}}{\partial Y}=\frac{1}{S_c}\frac{\partial^2 \overline{C}}{\partial Y^2}-\gamma \overline{C}+S_r\frac{\partial^2 \overline{T}}{\partial Y^2} \tag{15}$$

Also, the associate boundary conditions according to the problem are,

$$\left.\begin{array}{l} U=0,V=0,W=0,\overline{T}=1,\overline{C}=1 \quad \text{at } Y=0 \\ U=0,W=0,\overline{T}\to 0,\overline{C}\to 0 \qquad \text{as } Y\to\infty \end{array}\right\} \tag{16}$$

The physical quantities skin friction, Nusselt number, and Sherwood number in non-dimensional form of the present problem are presented respectively by the following expressions as

$$C_f=-\frac{1}{2\sqrt{2}}(G_r)^{-\frac{3}{4}}\left(\frac{\partial U}{\partial Y}\right)_{Y=0};N_u=-\frac{1}{2\sqrt{2}}(G_r)^{-\frac{3}{4}}\left(\frac{\partial \overline{T}}{\partial Y}\right)_{Y=0};S_h=-\frac{1}{2\sqrt{2}}(G_r)^{-\frac{3}{4}}\left(\frac{\partial \overline{C}}{\partial Y}\right)_{Y=0} \tag{17}$$

Stream function $\psi(X,Y)$ satisfies the continuity equation and associated with the velocity components as

$$U=\frac{\partial \psi}{\partial X},V=-\frac{\partial \psi}{\partial Y} \tag{18}$$

3 Calculation Technique

The nonlinear coupled partial differential equation (11) to (15) with respect to the boundary conditions (16) are solved numerically by using explicit finite difference method as below:

$$\frac{U_{i,j}-U_{i-1,j}}{\Delta X}+\frac{V_{i,j}-V_{i,j-1}}{\Delta Y}=0 \tag{19}$$

$$\frac{U'_{i,j}-U_{i,j}}{\Delta\tau}+U_{i,j}\left(\frac{U_{i,j}-U_{i-1,j}}{\Delta X}\right)+V_{i,j}\left(\frac{U_{i,j+1}-U_{i,j}}{\Delta Y}\right)=\left(1+\frac{1}{\beta}\right)\left(\frac{U_{i,j+1}-2U_{i,j}+U_{i,j-1}}{(\Delta Y)^2}\right)$$
$$+G_r\overline{T}_{i,j}+G_m\overline{C}_{i,j}-M\left(\frac{U_{i,j}+mW_{i,j}}{1+m^2}\right)-\left(1+\frac{1}{\beta}\right)k_pU_{i,j} \tag{20}$$

$$\frac{W'_{i,j}-W_{i,j}}{\Delta\tau}+U_{i,j}\left(\frac{W_{i,j}-W_{i-1,j}}{\Delta X}\right)+V_{i,j}\left(\frac{W_{i,j+1}-W_{i,j}}{\Delta Y}\right)=\left(1+\frac{1}{\beta}\right)\left(\frac{W_{i,j+1}-2W_{i,j}+W_{i,j-1}}{(\Delta Y)^2}\right)$$
$$-M\left(\frac{W_{i,j}-mU_{i,j}}{1+m^2}\right)-\left(1+\frac{1}{\beta}\right)k_pW_{i,j} \tag{21}$$

$$\frac{\overline{T}'_{i,j}-\overline{T}_{i,j}}{\Delta\tau}+U_{i,j}\frac{\overline{T}_{i,j}-\overline{T}_{i-1,j}}{\Delta X}+V_{i,j}\frac{\overline{T}_{i,j+1}-\overline{T}_{i,j}}{\Delta Y}=\left(\frac{1}{P_r}+R_a\right)\frac{\overline{T}_{i,j+1}-2\overline{T}_{i,j}+\overline{T}_{i,j-1}}{(\Delta Y)^2}$$
$$+\alpha\overline{T}_{i,j}+D_u\frac{\overline{C}_{i,j+1}-2\overline{C}_{i,j}+\overline{C}_{i,j-1}}{(\Delta Y)^2}+E_c\left(1+\frac{1}{\beta}\right)\left\{\left(\frac{U_{i,j+1}-U_{i,j}}{\Delta Y}\right)^2+\left(\frac{W_{i,j+1}-W_{i,j}}{\Delta Y}\right)\right\}^2$$
$$+\frac{E_cM}{(1+m^2)}(U_{i,j}^2+W_{i,j}^2)+Q\overline{C}_{i,j}+E_cMU_{i,j}^2 \tag{22}$$

$$\frac{\overline{C}'_{i,j}-C_{i,j}}{\Delta\tau}+U_{i,j}\frac{\overline{C}_{i,j}-\overline{C}_{i-1,j}}{\Delta X}+V_{i,j}\frac{\overline{C}_{i,j+1}-\overline{C}_{i,j}}{\Delta Y}=\frac{1}{S_c}\frac{\overline{C}_{i,j+1}-2\overline{C}_{i,j}+\overline{C}_{i,j-1}}{(\Delta Y)^2}-\gamma\overline{C}_{i,j}$$
$$+S_r\frac{\overline{T}_{i,j+1}-2\overline{T}_{i,j}+\overline{T}_{i,j-1}}{(\Delta Y)^2} \tag{23}$$

In this case, the associate boundary conditions according to the problem are,

$$\left.\begin{aligned}&U^n_{i,0}=0,\ V^n_{i,0}=0, W^n_{i,0}=0,\ \overline{T}^n_{i,0}=1,\ \overline{C}^n_{i,0}=1\\&U^n_{i,L}=0, W^n_{i,L}=0,\ \overline{T}^n_{i,L}\to 0,\ \overline{C}^n_{i,L}\to 0 \text{ where } L\to\infty\end{aligned}\right\} \tag{24}$$

Here i and j designate to the mesh points with X and Y coordinate respectively and the superscripts n represent a value of time, $\tau=n\Delta\tau$ where, n=0, 1, 2 …

4 Stability and Convergence Analysis

The stability conditions for the present problem are,

$$\left(1+\frac{1}{\beta}\right)\frac{2\Delta\tau}{(\Delta Y)^2}+\frac{M\Delta\tau}{1+m^2}+U\frac{\Delta\tau}{\Delta X}+|-V|\frac{\Delta\tau}{\Delta Y}+\left(1+\frac{1}{\beta}\right)\frac{K_p\Delta\tau}{2}\le 1 \tag{25}$$

$$\left(R_a+\frac{1}{P_r}\right)\frac{2\Delta\tau}{(\Delta Y)^2}+U\frac{\Delta\tau}{\Delta X}+|-V|\frac{\Delta\tau}{\Delta Y}-\frac{Q\Delta\tau}{2}\le 1 \tag{26}$$

$$\frac{1}{S_c}\frac{2\Delta\tau}{(\Delta Y)^2}+U\frac{\Delta\tau}{\Delta X}+|-V|\frac{\Delta\tau}{\Delta Y}+\frac{\gamma\Delta\tau}{2}\le 1 \tag{27}$$

Since the initial condition, U=V=0 at τ=0. So, the equations (25) to (27) present $P_r\ge$ 0.04 and $S_c\ge$0.03 respectively.

Therefore, the convergence criteria of the present problem are $P_r\ge$ 0.63 and $S_c\ge$0.20.

5 Results and Discussion

In this paper, the explicit finite difference method is used to obtain the results of the problem. The approximate solutions are obtained for various parameters for the purpose of discussing the results of the problem. To observe the physical situation of the problem, the numerical values of the non-dimensional primary velocity, secondary velocity, temperature, concentration, skin friction, Nusselt number, Sherwood number, streamlines and isotherms for vertical plate within the boundary conditions are computed. The numerical results have been obtained for different values of Casson parameter (β), Magnetic parameter (M), Hall parameter (H), Eckert number (E_c), Permeability of porous medium (K_p), Schmidt number (S_c), Prandtl number (P_r), Chemical reaction parameter (γ), Grashof number (G_r), modified Grashof number (G_m), Dufour number (D_u) and Radiation parameter (R_a). For numerical results it has been used M=0.50, P_r=0.63, S_c=0.30, R_a=0.20, E_c=0.01, D_u=0.10, m=0.50, β=0.20 and γ=0.50. These values are treated as common throughout the study in respective Figs and Table 1.

Figs. 2 and 3 represent the primary velocity and secondary velocity respectively for different values of Casson parameter. In this observation, the numerical values of velocities are obtained as 0.59663, 0.56876,

0.52823, 0.46387 and 0.34490 for β=0.20, 0.40, 0.60, 0.80 and 1.00 respectively at Y=1.33779. It is observed that from Fig. 2 primary velocity decreases 59.49%, 32.50%, 20.25%, and 13.95% for β=0.20 to β=0.40, β=0.40 to β=0.60, β=0.60 to β =0.80 and β=0.80 to β=1.00. On the other hand secondary velocity decreases 0.63%, 0.33%, 0.191%, and 0.12% for β =0.20 to β =0.40, β =0.40 to β=0.60, β=0.60 to β =0.80 and β =0.80 to β =1.00 respectively which occurs at time τ=1. Physically, by increasing the Casson parameter which reduces the yield stress suppresses the fluid velocity i.e. it produces resistance force in the fluid flow. The influence of chemical reaction parameter on primary velocity, secondary velocity and concentration are shown in Figs. 4 to 6 respectively. From the Fig. 4 it is carried out that the primary velocity decreases 6.53% from γ=0.50 to γ=1.50, 4.12 % from γ=1.50 to γ=2.50, 2.78 % from γ=2.50 to γ=3.50 and 1.99% for γ=3.50 to γ=4.50. The velocity attains its maximum value at Y= 1.33779. Also, from Fig. 5 secondary velocity decreases 0.29%, 0.18%, 0.12% and 0.08% from 0.50 to 1.50, 1.50 to 2.50, 2.50 to 3.50 and 3.50 to 4.50 respectively for increasing of chemical reaction parameter γ and concentration profiles decreases 0.78%, 0.35%, 0.17% and 0.08% due to increase for γ from γ=1.50 to γ=2.50, 2.78 % from γ=2.50 to γ=3.50 and 1.99% for γ=3.50 to γ=4.50 in the Fig. 6. It is notated that chemical reaction parameter leads to downfall of velocity and concentration because the positive values of chemical reaction parameter (γ< 0) predicts the effects of destructive chemical reaction on the concentration field. Physically for generative case, chemical reaction γ takes place without creating much disturbance whereas in the case of destructive chemical reaction is much larger. Due to this fact molecular motion in the case of (γ < 0) is quite larger which finally results in an increase in the mass transport phenomenon.

The effects of different values of Grashof number on primary velocity and secondary velocity are shown in Figs. 7 and 8 respectively. From Figs. 7 and 8 we observed that primary and secondary velocity profiles are increasing respectively as Grashof number but there is no effect on temperature and concentration distributions. The thermal Grashof number which signifies the relative effect of the thermal buoyancy force in the boundary layer. Due to this enhancement of thermal buoyancy force which acting on the fluid particles for gravitational force that increases the primary and secondary velocity.

For various values of permeability of porous medium K_p on primary velocity and secondary are delimitated in Figs. 9 and 10 respectively. From Figs. 9 and 10 it is observed that primary velocity profiles are decreasing 4.6%, 3.6%, 2.8% and 2.2% as permeability of porous medium K_p changes as 0.50 to 1.50, 1.50 to 2.50, 2.50 to 3.50 and 3.50 to 4.50 respectively and secondary velocity decreasing 0.41%, 0.26%, 0.17% and 0.12% as permeability of porous medium K_p changes from 0.50 to 1.50, 1.50 to 2.50, 2.50 to 3.50 and 3.50 to 4.50 respectively which occurs at time τ=1 with the increasing of porous medium permeability K_p. Generally, the permeability of porous medium K_p which increases the resistive force. Due to this resistive force, primary and secondary velocity profiles are decreasing with the increasing of permeability of porous medium K_p. For different values of Prandtl number P_r on primary velocity, secondary velocity and temperature are analyzed in Figs. 11 to 13 respectively. In this case velocity is decreasing with the increasing of Prandtl number which is observed from Figs. 11 and 12, primary and secondary velocity decreases with the increases of Prandtl number. Also, temperature distributions decreases 0.25%, 0.07%, 0.002% and 0.0009% at Y=0.35452 for P_r=0.63 to P_r=0.71, P_r=0.71 to P_r=1.00, P_r=1.00 to P_r=7.00 and P_r=7.00 to P_r=11.25 which are shown in Fig. 13. Naturally, this is due to the fluid with high Prandtl number have greater viscosity, which decreases thermal boundary layer thickness i.e. for decreasing thermal boundary layer, heat transfer is reduced.

Primary velocity, secondary velocity and temperature are shown in Figs. 14 to 16 respectively for different values of Radiation parameter R_a. From Figs. 14 to 16 it is noticed that there is an increment in the primary velocity, secondary velocity and temperature profiles for the increase of Radiation parameter R_a. This may happen due to an increase of Radiation parameter R_a which enhance the thermal boundary layer. But, on the other hand there is no effect on concentration distributions. Also we observed from Fig. 17 concentration distributions decreases by 1.17%, 0.83%, 0.68% and 0.67% as Schmidt number S_c changes as 0.30 to 0.60, 0.60 to 0.78, 0.78 to 0.94 and 0.94 to 1.00 respectively which occurs at time τ=1. It is true by physically that the Schmidt number S_c increases, the concentration decreases. It happens for increasing concentration which increases the density of the fluid as well as concentration buoyancy force in the fluid. The influence of Casson parameter β on streamlines and isotherms are represented in Figs. 18 and 19. The momentum

boundary layer thickness decreases and thermal boundary layer thickness decreases due to increase of Casson parameter. Also, the impact of radiation parameter R_a on streamlines and isotherms are represented in Figs. 20 and 21. Here, we observed that momentum boundary layer thickness and thermal boundary layer thickness are increasing due to the increase of radiation parameter from R_a=0.20 to R_a=0.40.

Table 1 represent the variation of different parameters on skin friction, Nusselt number and Sherwood number for Casson fluid. For various values of permeability of porous medium K_p on skin friction, Nusselt number and Sherwood number are delimitated in Table 1. It is observed that skin friction coefficient decreases by 0.65%, 0.55%, 0.47% and 0.41% as permeability of porous medium K_p changes from 0.50 to 1.50, 1.50 to 2.50, 2.50 to 3.50 and 3.50 to 4.50 respectively at Y=0.57750. Also, Nusselt number increases by 0.14%, 0.36%, 0.005% and 0.005% as permeability of porous medium K_p changes from 0.50 to 1.50, 1.50 to 2.50, 2.50 to 3.50 and 3.50 to 4.50 respectively at Y=0.57750. Physically, permeability of porous medium increases total heat transfer due to the increasing of Nusselt number. Skin friction coefficient decreases to 4.39%, 3.28%, 0.587% and 0.09% but Nusselt number increases to 23.75%, 20.10%, 6.17% and 1.76% at Y=0.35452 as Prandtl number changes from 0.63 to 0.71, 0.71 to 1.00, 1.00 to 7.00 and 7.00 to 11.25 respectively. It is clear that, skin friction coefficient increases but Nusselt number decreases as Radiation parameter R_a changes from 0.20 to 0.50, 0.50 to 0.80, 0.80 to 1.00 and 1.00 to 1.50 at Y= 0.5560. On the other hand skin friction and Nusselt number decreases but Sherwood number increases from S_c=0.30 to S_c=0.60, S_c=0.60 to S_c=0.78, S_c=0.78 to S_c=0.94 and S_c=0.94 to S_c=1.00 respectively. This is fact that, Schmidt number increase the convective mass transfer rate due to increases of Schmidt number. We observed from Table 1 skin friction coefficient decreases 1.10%, 1.05%, 0.95% and 0.41% as magnetic parameter changes from M=0.50 to M=0.70, M=0.70 to M=0.90, M=0.90 to M=1.50 and M=1.50 to M=2.50 respectively but Nusselt number increases due to increasing of magnetic parameter. From Table 1 we conclude that skin friction coefficient increases by 6.30%, 4.20%, 3.04% and 2.32% as Casson parameter changes from 0.2 to 0.40, 0.40 to 0.60, 0.60 to 0.80 and 0.80 to 1.00 respectively but Nusselt number decreases. In this case, total heat transfer increase due to the increase of Casson parameter. It is noted that increasing in Chemical reaction parameter γ increases the skin friction coefficient and Sherwood number but Nusselt number decreases. Due to an increase of chemical reaction parameter i.e. an increase in the interfacial mass transfer causes the improvement of the Sherwood number and skin friction coefficient but decrease Nusselt number. Skin friction coefficient increases by 0.29%, 0.22%, 0.20% and 0.16% as Grashof number changes as 5 to 10, 10 to 15, 15 to 20 and 20 to 25 respectively but Nusselt number and Sherwood number decreases for increasing Grashof number.

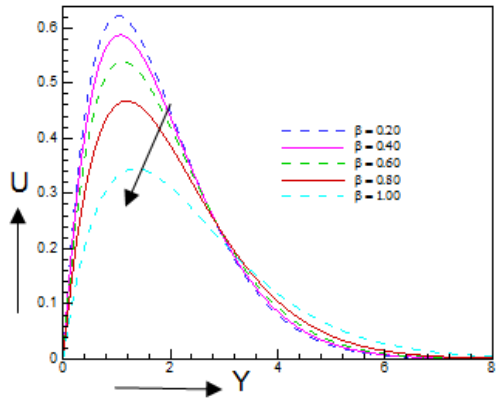

Fig. 2. Primary velocity profiles for different values of β against Y when M=0.50, P_r=0.63, S_c=0.30, R_a=0.20, E_c=0.01, D_u=0.10, m=0.50 and γ=0.50

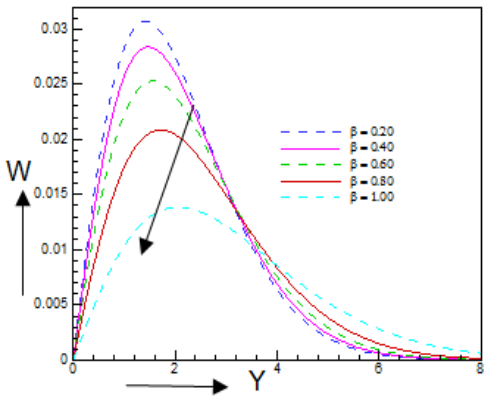

Fig. 3. Secondary velocity profiles for different values of β against Y when M=0.50, P_r=0.63, S_c=0.30, R_a=0.20, E_c=0.01, D_u=0.10 and γ=0.50

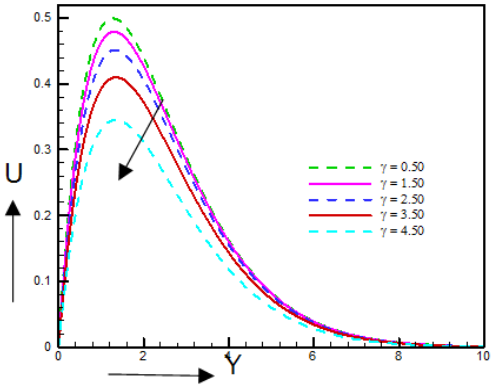

Fig. 4. Primary velocity profiles for different values of Chemical reaction parameter γ against Y when M=0.50, P_r=0.63, S_c=0.30, R_a=0.20, E_c=0.01, D_u=0.10, m=0.50 and β=0.20

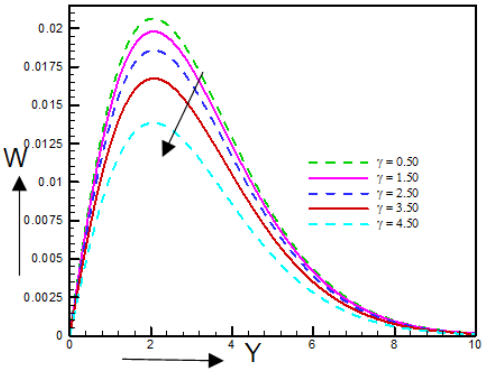

Fig. 5. Secondary velocity profiles for different values of Chemical reaction parameter γ against Y when M=0.50, P_r=0.63, S_c=0.30, R_a=0.20, E_c=0.01, D_u=0.10, m=0.50 and β=0.20

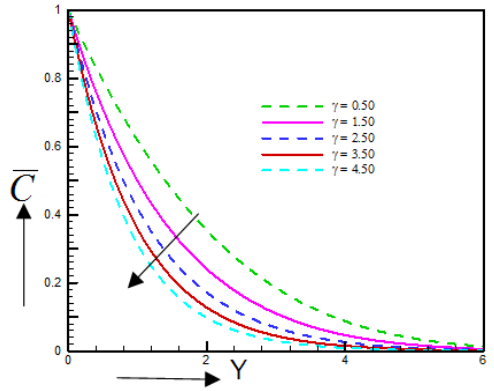

Fig. 6. Concentration profiles for different values of Chemical reaction parameter γ against Y when M=0.50, P_r=0.63, S_c=0.30, R_a=0.20, E_c=0.01, D_u=0.10, m=0.50 and β=0.20

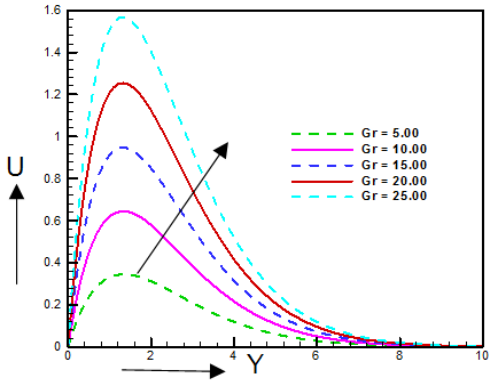

Fig. 7. Primary velocity profiles for different values of Grashof number G_r against Y when M=0.50, P_r=0.63, S_c=0.30, R_a=0.20, E_c=0.01, D_u=0.10, m=0.50, β=0.20 and γ=0.50

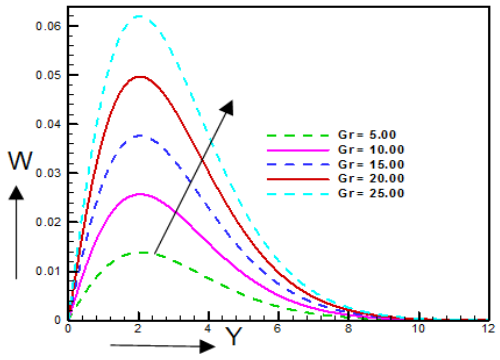

Fig. 8. Secondary velocity profiles for different values of Grashof number G_r against Y when M=0.50, P_r=0.63, S_c=0.30, R_a=0.20, E_c=0.01, D_u=0.10, m=0.50, β=0.20 and γ=0.50

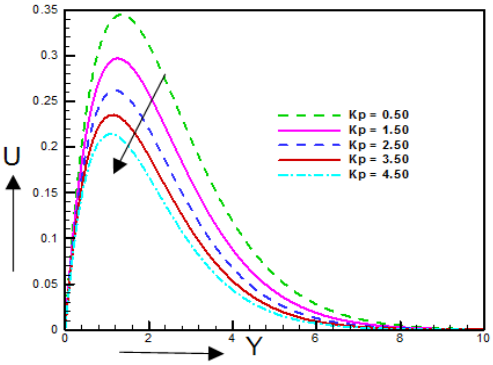

Fig. 9. Primary velocity profiles for different values of Permeability of porous medium K_p against Y when M=0.50, P_r=0.63, S_c=0.30, R_a=0.20, E_c=0.01, D_u=0.10, m=0.50, β=0.20 and γ=0.50

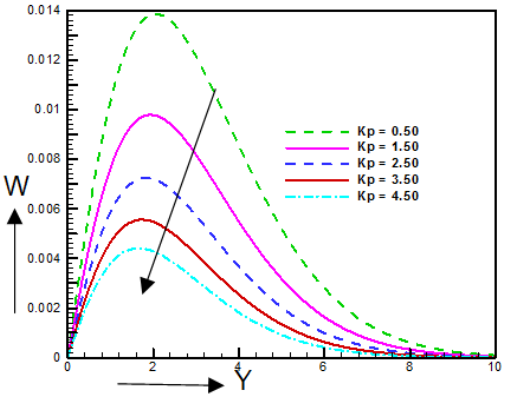

Fig. 10. Secondary velocity profiles for different values of K_p against Y when M=0.50, P_r=0.63, R_a=0.20, E_c=0.01, m=0.50, β=0.20 and γ=0.50

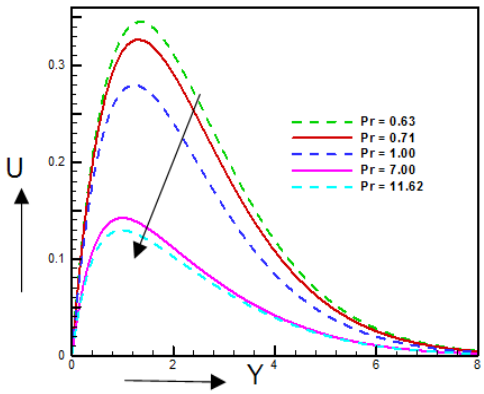

Fig. 11. Primary velocity profiles for different values of P_r against Y when M=0.50, S_c=0.30, E_c=0.01, D_u=0.10, m=0.50, β=0.20 and γ=0.50

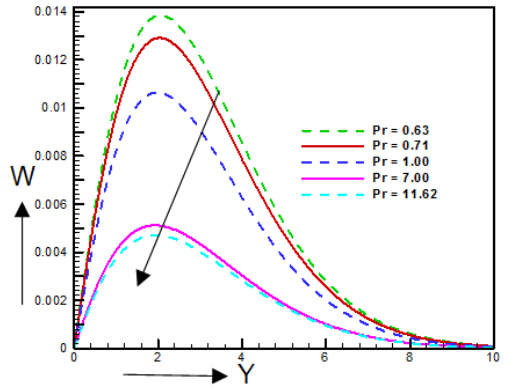

Fig. 12. Secondary velocity profiles for different values of Prandtl number P_r against Y when M=0.50, S_c=0.30, R_a=0.20, E_c=0.01, D_u=0.10, m=0.50, β=0.20 and γ=0.50

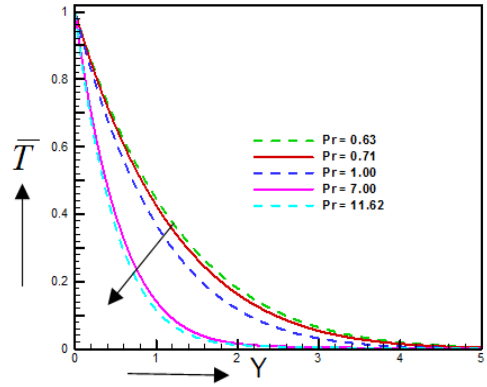

Fig. 13. Temperature profiles for different values of Prandtl number P_r against Y when M=0.50, S_c=0.30, R_a=0.20, E_c=0.01, D_u=0.10, m=0.50, β=0.20 and γ=0.50

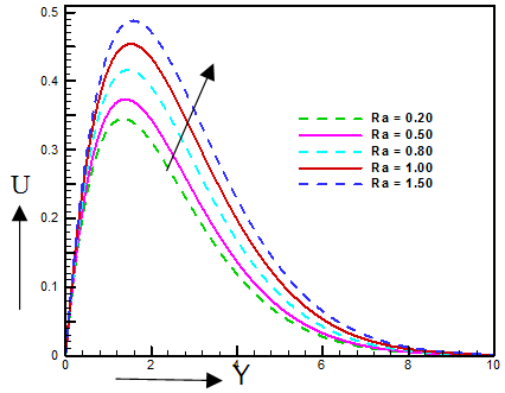

Fig. 14. Primary velocity profiles for different values of Radiation parameter R_a against Y when M=0.50, P_r=0.63, S_c=0.30, E_c=0.01, D_u=0.10, m=0.50, β=0.20 and γ=0.50

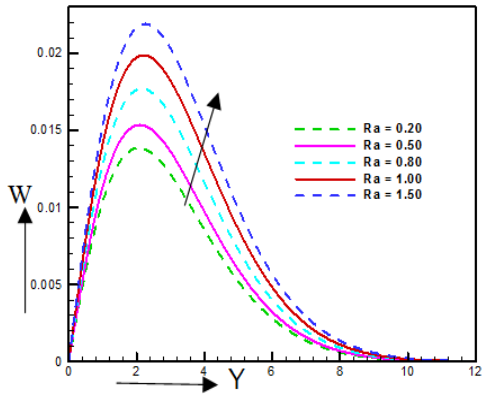

Fig. 15. Secondary velocity profiles for different values of Radiation parameter R_a against Y when M=0.50, P_r=0.63, S_c=0.30, E_c=0.01, D_u=0.10, m=0.50, β=0.20 and γ=0.5

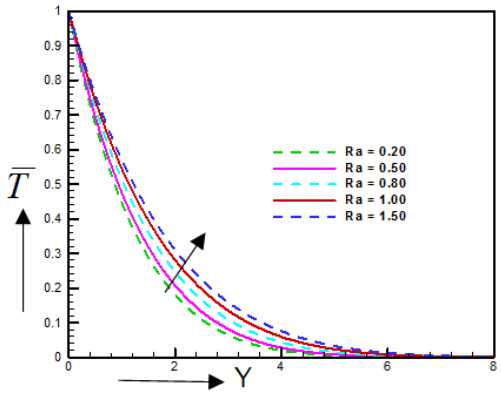

Fig. 16. Temperature profiles for different values of Radiation parameter R_a against Y when M=0.50, P_r=0.63, S_c=0.30, E_c=0.01, D_u=0.10, m=0.50, β=0.20 and γ=0.50

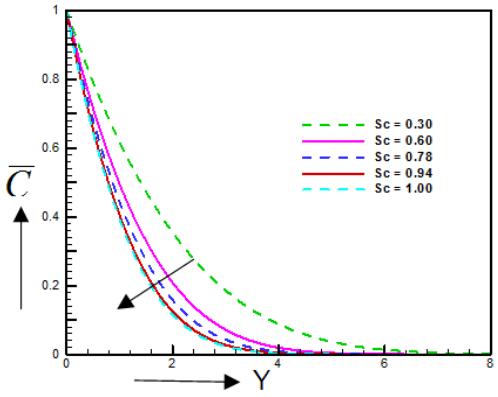

Fig. 17. Concentration profiles for different values of Schmidt number S_c against Y when M=0.50, P_r=0.63, R_a=0.20, E_c=0.01, D_u=0.10, m=0.50, β=0.20 and γ=0.50

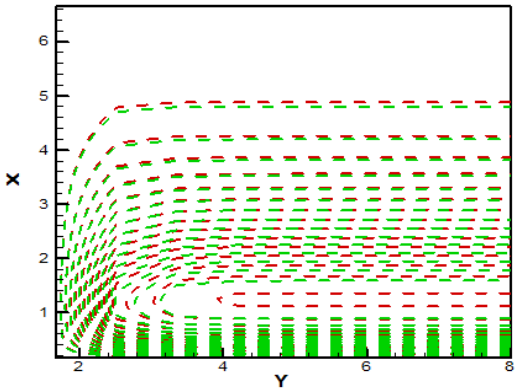

Fig. 18. Streamlines for β=0.20 (red dashed line) and β=0.40 (green dashed line)

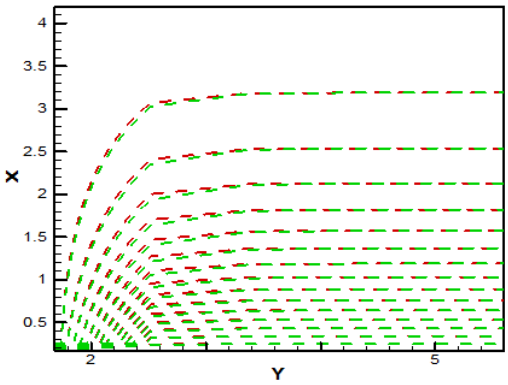

Fig. 19. Isotherms for β=0.20 (red dashed line) and β=0.40 (green dashed line)

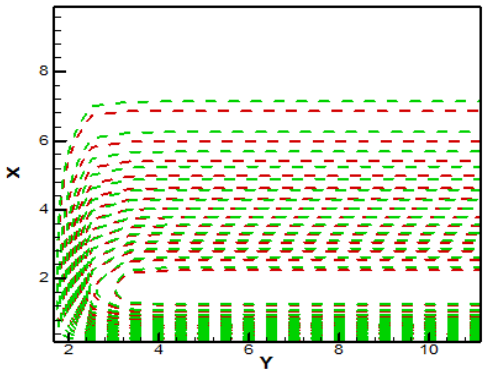

Fig. 20. Streamlines for R_a=0.20 (red dashed line) and R_a =0.40 (green dashed line)

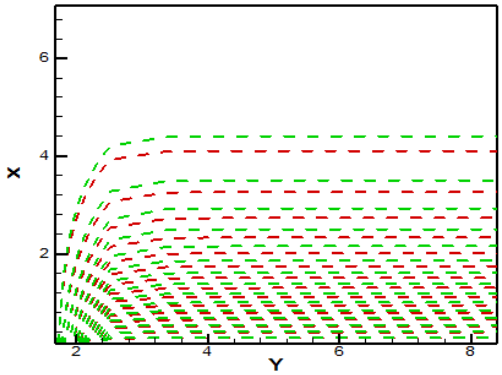

Fig. 21. Isotherms for R_a=0.20 (red dashed line) and R_a =0.40 (green dashed line)

Table 1. Variation of different parameters on skin friction, Nusselt number and Sherwood number for Casson fluid

K_p	P_r	R_a	S_c	M	β	γ	G_r	C_f	N_u	S_h
0.50	0.63	0.20	0.30	0.50	0.20	0.50	5.00	0.12123	0.36731	0.23310
1.50	0.63	0.20	0.30	0.50	0.20	0.50	5.00	0.11478	0.36738	0.23310
2.50	0.63	0.20	0.30	0.50	0.20	0.50	5.00	0.10930	0.36744	0.23310
3.50	0.63	0.20	0.30	0.50	0.20	0.50	5.00	0.10460	0.36749	0.23310
4.50	0.63	0.20	0.30	0.50	0.20	0.50	5.00	0.10051	0.36754	0.23310
0.50	0.63	0.20	0.30	0.50	0.20	0.50	5.00	0.12160	0.35241	0.22797
0.50	0.71	0.20	0.30	0.50	0.20	0.50	5.00	0.11809	0.37139	0.22797
0.50	1.00	0.20	0.30	0.50	0.20	0.50	5.00	0.10861	0.42965	0.22797
0.50	7.00	0.20	0.30	0.50	0.20	0.50	5.00	0.07397	0.79990	0.22797
0.50	11.62	0.20	0.30	0.50	0.20	0.50	5.00	0.06983	0.87478	0.22797
0.50	0.63	0.20	0.30	0.50	0.20	0.50	5.00	0.11974	0.35555	0.22219
0.50	0.63	0.50	0.30	0.50	0.20	0.50	5.00	0.12493	0.32913	0.22219
0.50	0.63	0.80	0.30	0.50	0.20	0.50	5.00	0.13225	0.29576	0.22219
0.50	0.63	1.00	0.30	0.50	0.20	0.50	5.00	0.13839	0.27085	0.22219
0.50	0.63	1.50	0.30	0.50	0.20	0.50	5.00	0.14366	0.25135	0.22219
0.50	0.63	0.20	0.30	0.50	0.20	0.50	5.00	0.11889	0.35705	0.22329
0.50	0.63	0.20	0.60	0.50	0.20	0.50	5.00	0.11698	0.35363	0.31579
0.50	0.63	0.20	0.78	0.50	0.20	0.50	5.00	0.11633	0.35183	0.36007
0.50	0.63	0.20	0.94	0.50	0.20	0.50	5.00	0.11588	0.35034	0.39529
0.50	0.63	0.20	1.00	0.50	0.20	0.50	5.00	0.11546	0.35030	0.40864
0.50	0.63	0.20	0.30	0.50	0.20	0.50	5.00	0.11726	0.36075	0.22686
0.50	0.63	0.20	0.30	0.70	0.20	0.50	5.00	0.11505	0.36078	0.22686
0.50	0.63	0.20	0.30	0.90	0.20	0.50	5.00	0.11296	0.36080	0.22686
0.50	0.63	0.20	0.30	1.50	0.20	0.50	5.00	0.10730	0.36087	0.22686
0.50	0.63	0.20	0.30	2.50	0.20	0.50	5.00	0.10320	0.36092	0.22686
0.50	0.63	0.20	0.30	0.50	0.20	0.50	5.00	0.11849	0.35776	0.22398
0.50	0.63	0.20	0.30	0.50	0.40	0.50	5.00	0.18148	0.35758	0.22398
0.50	0.63	0.20	0.30	0.50	0.60	0.50	5.00	0.22348	0.35750	0.22398
0.50	0.63	0.20	0.30	0.50	0.80	0.50	5.00	0.25391	0.35745	0.22398
0.50	0.63	0.20	0.30	0.50	1.00	0.50	5.00	0.27711	0.35741	0.22398
0.50	0.63	0.20	0.30	0.50	0.20	0.50	5.00	0.11950	0.35598	0.22225
0.50	0.63	0.20	0.30	0.50	0.20	1.50	5.00	0.14280	0.35261	0.30400
0.50	0.63	0.20	0.30	0.50	0.20	2.50	5.00	0.16257	0.34952	0.37442
0.50	0.63	0.20	0.30	0.50	0.20	3.50	5.00	0.17976	0.34667	0.43634
0.50	0.63	0.20	0.30	0.50	0.20	4.50	5.00	0.19501	0.34402	0.49176
0.50	0.63	0.20	0.30	0.50	0.20	0.50	5.00	0.11808	0.35848	0.22468
0.50	0.63	0.20	0.30	0.50	0.20	0.50	10.00	0.13273	0.21208	0.13359
0.50	0.63	0.20	0.30	0.50	0.20	0.50	15.00	0.14417	0.15519	0.09856
0.50	0.63	0.20	0.30	0.50	0.20	0.50	20.00	0.15360	0.12364	0.07944
0.50	0.63	0.20	0.30	0.50	0.20	0.50	25.00	0.16174	0.10303	0.06719

Table 2. Comparison of the accuracy of the present results with the previous results by Raju et al. [2]

Previous results by Raju et al. [2]							Our present results					
Increased parameters	U	T	C	**Skin fri.**	**Nusl. Num.**	**Sher. Num.**	U	$\overline{T}$	$\overline{C}$	**Skin fri.**	**Nusl. Num.**	**Sher. Num.**
M				Dec	Inc					Dec	Inc	
γ	Dec		Dec	Dec	Dec	Inc	Dec		Dec	Inc	Dec	Inc
K_p							Dec			Dec	Inc	
P_r	Dec	Dec		Dec	Inc		Dec	Dec		Dec	Inc	
R_a	Inc	Inc		Inc	Dec		Inc	Inc		Inc	Dec	
S_c									Dec	Dec	Dec	Inc
β							Dec			Inc	Dec	
G_r	Inc						Inc			Inc	Dec	Dec

6 Conclusion

From the present numerical investigation, following conclusions have been drawn:

1) It is noticed that Grashof number increases the primary velocity, secondary velocity and skin friction coefficient but decreases the Nusselt number and Sherwood number.
2) An increase in Chemical reaction parameter increases the skin-friction coefficient.
3) It is observed that Permeability of porous medium decreases the primary velocity, secondary velocity and skin friction coefficient but increses Nusselt number.
4) In view of that Prandtl number decreases the primary velocity, secondary velocity and skin friction coefficient but increases only Nusselt number.
5) Radiation parameter increases the primary velocity, secondary velocity and skin friction coefficient but decreases the Nusselt number.
6) Primary velocity profiles decreases with the increase of Magnetic Parameter.

Competing Interests

Authors have declared that no competing interests exist.

References

[1] Sojoudi A, Mazloomi A, Saha SC, Gu YT. Similarity solutions for flow and heat transfer of non-Newtonian fluid over a stretching surface. Journal of Applied Mathematics; 2014. Article ID 718319, Pages 8.

[2] Raju CSK, Sandeep N, Sugunamma V, Babu MJ, Reddy JVR. Heat and mass transfer in magneto-hydrodynamic Casson fluid over an exponentially permeable stretching surface. Engineering Science and Technology, an International Journal. 2016;19:45-52.

[3] Kataria HR, Patel HR. Soret and heat generation effects on MHD Casson fluid flow past an oscillating vertical plate embedded through porous medium. Alexandria Engineering Journal. 2016;55:2125-2137.

[4] Oyelakin IS, Mondal S, Sibanda P. Unsteady Casson nanofluid flow over a stretching sheet with thermal radiation, convective and slip boundary conditions. Journal of the Nigerian Mathematical Society. 2015;34:11-31.

[5] Animasaun IL. Effects of thermophoresis, variable viscosity and thermal conductivity on free convective heat and mass transfer of non-darcian MHD dissipative Casson fluid flow with suction and nth order of chemical reaction. Journal of the Nigerian Mathematical Society. 2015;34:11-31.

[6] Animasaun IL, Adebile EA, Fagbade AI. Casson fluid flow with variable thermo-physical property along exponentially stretching sheet with suction and exponentially decaying internal heat generation using the homotopy analysis method. Journal of the Nigerian Mathematical Society. 2016;35:11-17.

[7] Ahmed N, Khan U, Khan SI, Bano S, Mohyud-Din ST. Effects on magnetic field in squeezing flow of a Casson fluid between parallel plates. Journal of King Saud University Science. 2017;29:119-125.

[8] Sulochana C, Ashwinkumar GP, Sandeep NI. Similarity solution of 3D Casson nanofluid flow over a stretching sheet with convective boundary conditions. Journal of the Nigerian Mathematical Society. 2016;35:128-141.

[9] Hossain MD, Samad MA, Alam MM. MHD free convection and mass transfer flow through a vertical oscillatory porous plate with hall, ion-slip currents and heat source in a rotating system. Procedia Engineering. 2015;105:56-63.

[10] Sarkar BC, Das S, Jana. Hall effects on unsteady MHD free convective flow past an accelerated moving vertical plate with viscous and joule dissipations. International Journal of Computer Applications. 2013;70:0975-8887.

[11] Seth GS, Sarkar S, Hussain SM. Effects of hall current, radiation and rotation on natural convection heat and mass transfer flow past a moving vertical plate. Ain Shams Engineering Journal. 2014;5:489-503.

[12] Pattnaik JR, Dash GC, Singh S. Diffusion- thermo effect with hall current on unsteady hydromagnetic flow past an infinite vertical porous plate. Alexandria Engineering Journal. 2017;56:13-25.

[13] Hossain MA, Munir MS, Gorla RRS. Combined convection from a vertical flat plate with temperature dependent viscosity and thermal conductivity. International Journal of Fluid Mechanics Research. 2002;29:6.

[14] Tamoor M, Waqas M, Khan MI, Alsaedi A, Hayat T. Magneto-hydrodynamic flow of Casson fluid cylinder. Results in Physics. 2017;7.

[15] Das S, Guchhait SK, Jana RN, Makinde OD. Hall effects on an unsteady magneto-convection and radiative heat transfer past a porous plate. Alexandria Engineering Journal. 2016;55:1321-1331.

[16] Mishra SR, Baag S, Mohapatra DK. Chemical reaction and Soret effects on hydromagnetic micropolar fluid along a stretching sheet. Engineering Science and Technology, an International Journal. 2016;19:1919-1928.

[17] Ahmed T, Alam MM. Finite difference solution of MHD mixed convection flow with heat generation and chemical reaction. Procedia Engineering. 2013;56:149-156.

[18] Kataria HR, Patel HR. Radiation and chemical reaction effects on MHD Casson fluid flow past an oscillating vertical plate embedded in porous medium. Alexandria Engineering Journal. 2016;55:583-595.

[19] Narayanan PVS. Effects of variable permeability and radiation absorption on magneto hydrodynamic (MHD) mixed convective flow in a vertical wavy channel with traveling thermal waves. Propulsion and Power Research. 2015;4(3):150-160.

[20] Tripathy RS, Dash GC, Mishra SR, Baag S. Chemical reaction effect on MHD free convective surface over a moving vertical plate through porous medium. Alexandria Engineering Journal. 2015;54:673-679.

Peer-review history:
The peer review history for this paper can be accessed here (Please copy paste the total link in your browser address bar)
http://sciencedomain.org/review-history/19926